Cancer-associated fibroblasts lead tumor invasion through integrin-β3–dependent fibronectin assembly

Youmna Attieh, Andrew G Clark, Carina Grass, Sophie Richon, Marc Pocard, Pascale Mariani, Nadia Elkhatib, Timo Betz, Basile Gurchenkov, Danijela Matic Vignjevic

Cancer-associated fibroblasts lead tumor invasion through integrin-β3–dependent fibronectin assembly

Youmna Attieh,[1,2] Andrew G. Clark,[1] Carina Grass,[1,3] Sophie Richon,[1] Marc Pocard,[4] Pascale Mariani,[5] Nadia Elkhatib,[6] Timo Betz,[7] Basile Gurchenkov,[1] and Danijela Matic Vignjevic[1]

[1]Institut Curie, Paris Sciences et Lettres Research University, Centre National de la Recherche Scientifique, UMR 144, Paris, France
[2]Sorbonne Universités, University Pierre and Marie Curie, University of Paris 6, Institute of Doctoral Studies, Paris, France
[3]Department of Biochemistry, Technische Universitaet Munich, Munich, Germany
[4]Chirurgie digestive et cancérologique, Hôpital Lariboisière, Université Paris Diderot, Sorbonne Paris Cité, Assistance Publique Hôpitaux de Paris, Paris, France
[5]Department of Surgery, Institut Curie, Paris Sciences et Lettres Research University, Paris and Saint Cloud, France
[6]Institut National de la Santé et de la Recherche Médicale U1170, Gustave Roussy Institute, Université Paris-Saclay, Villejuif, France
[7]Center for Molecular Biology of Inflammation, Cells-in-Motion Cluster of Excellence, Institute of Cell Biology, Münster University, Münster, Germany

Cancer-associated fibroblasts (CAFs) are the most abundant cells of the tumor stroma. Their capacity to contract the matrix and induce invasion of cancer cells has been well documented. However, it is not clear whether CAFs remodel the matrix by other means, such as degradation, matrix deposition, or stiffening. We now show that CAFs assemble fibronectin (FN) and trigger invasion mainly via integrin-αvβ3. In the absence of FN, contractility of the matrix by CAFs is preserved, but their ability to induce invasion is abrogated. When degradation is impaired, CAFs retain the capacity to induce invasion in an FN-dependent manner. The level of expression of integrins αv and β3 and the amount of assembled FN are directly proportional to the invasion induced by fibroblast populations. Our results highlight FN assembly and integrin-αvβ3 expression as new hallmarks of CAFs that promote tumor invasion.

Introduction

Metastasis formation is a complex multistep process that requires cancer cells to move from their tissue of origin to neighboring and distant organs (Joyce and Pollard, 2009; Wirtz et al., 2011). Through their journey, cancer cells cooperate with the tumor microenvironment, which promotes their invasion (Mueller and Fusenig, 2004; Joyce and Pollard, 2009). Cancer-associated fibroblasts (CAFs) are the most abundant cells in the tumor microenvironment (Kalluri and Zeisberg, 2006). They are a unique cell population, as they can modulate cancer cell invasion directly by secreting proinvasive stimuli and indirectly by remodeling the matrix (Attieh and Vignjevic, 2016).

During the progression of carcinoma, after breaching of the basement membrane, cancer cells reach the tumor stroma, encountering CAFs and the ECM. At this stage, the influence of CAFs on tumor invasion is still debated (Kalluri, 2016): it has been shown that depleting CAFs from the stroma induces tumor invasion (Özdemir et al., 2014; Rhim et al., 2014), but most studies agree that an enrichment in CAFs stimulates cancer cell invasion (De Wever et al., 2004; Orimo et al., 2005, Gaggioli et al., 2007; Goetz et al., 2011). There is also disagreement concerning the mechanism by which CAFs act: Do they enhance the invasive capacity of cancer cells through diffusible molecules (De Wever et al., 2004; Orimo et al., 2005)? Or is their physical presence required to contract and align the matrix (Gaggioli et al., 2007; Goetz et al., 2011; Sanz-Moreno et al., 2011; Calvo et al., 2013), facilitating cancer cell invasion (Riching et al., 2014)?

Most new studies highlight the importance of contractility in CAFs in stimulating invasion. However, the ability of CAFs to remodel the matrix by other mechanisms (degradation, stiffening, or deposition of new ECM) and the interdependence between those mechanisms have been poorly studied. For example, highly contractile cells are characterized by stable and long-lived fibrillar adhesions that deposit and assemble new ECMs (Zaidel-Bar et al., 2007). Therefore, ECM deposition by CAFs is a direct consequence of their contractility. The tumor stroma is known to be enriched in matrix proteins like fibronectin (FN) and tenascin C that favor tumor progression (De Wever et al., 2004; Oudin et al., 2016), but it is still not known which of the two functions, contractility or matrix deposition, is responsible for cancer cell invasion.

Here, we investigate how CAFs induce invasion of cancer cells through the ECM. Using a combination of pharmacological and genetic perturbations, we modulated the ability of CAFs to contract, deposit, and degrade the matrix. We found that FN assembly by CAFs via integrin-αvβ3 is critical to stimulate cancer cell invasion.

Correspondence to Youmna Attieh: youmna.attie@curie.fr

Abbreviations used: AA, antibiotic–antimycotic; α-SMA, α smooth muscle actin; CAF, cancer-associated fibroblast; CAFcm, CAF-conditioned media; CAFdm, CAF's diffusible molecules; FAP, fibroblast activation protein; FN, fibronectin; MMP, matrix metalloproteinase; NAFs, noncancer-associated fibroblasts; PDGFR-β, PDGF receptor β.

The Rockefeller University Press
J. Cell Biol. Vol. 216 No. 11 3509–3520
https://doi.org/10.1083/jcb.201702033

Results and discussion

The physical presence of CAFs in the matrix is required to induce cancer cell invasion

To investigate the role of CAFs in cancer invasion, we isolated CAFs and noncancer-associated fibroblasts (NAFs) from the tumor and the neighboring healthy tissue of the colon of patients, respectively, ending with a couple of NAFs and CAFs per patient. We characterized all cell populations using markers of activated fibroblasts (see Materials and methods; Fig. S1 A). In all patients, CAFs and NAFs expressed α smooth muscle actin (α-SMA), fibroblast activation protein (FAP), and PDGF receptor β (PDGFR-β; Fig. S1 A), indicating that even though they were isolated from seemingly healthy tissue, NAFs exhibit features of activated fibroblasts.

To assess the role of CAFs and NAFs in cancer cell invasion of the ECM, we embedded spheroids of CT26 cancer cells in a collagen I matrix either alone or together with CAFs or NAFs (Fig. 1 A). This 3D model recapitulates the scenario of a tumor mass invading the stroma. The invasion capacity of cancer cells was quantified using a custom analysis software 3 d after embedding (see Materials and methods; Fig. 1 B). CT26 is an invasive cancer cell line (Geraldo et al., 2013), and in this assay, cells invaded the collagen matrix even when cultured alone (Fig. 1, A and C). However, in the presence of fibroblasts, the invasion of cancer cells was further enhanced, as previously shown for other noninvasive cancer cell lines (Fig. 1, A and C; Gaggioli et al., 2007; Goetz et al., 2011; Labernadie et al., 2017). CAFs were also more potent in increasing invasion compared with their paired NAFs (Fig. 1, A and C). To validate that this phenotype was not caused by an increased attraction of CAFs compared with NAFs by the tumor, we quantified the number of fibroblasts and their distance from the spheroid. Both CAFs and NAFs accumulated at 50–120 µm from the spheroid edge, and they were found in similar numbers (Fig. 1 D). This suggests that the increased invasion index in the presence of CAFs is most likely caused by an increased potential to secrete proinvasive diffusible molecules or to remodel the matrix.

We next investigated whether CAFs have to be present in collagen gels to stimulate invasion of cancer cells or whether their diffusible molecules are sufficient. In one of the conditions, we added CAF-conditioned media (CAFcm) to spheroids embedded in collagen. Alternatively, we cultured CAFs in the distant presence of cancer cell spheroids (CAF's diffusible molecules [CAFdm]); in the latter condition, CAFs were not present in the matrix to remodel it, but the secretome cross talk of both cell types was maintained (Fig. 1 E, schemes). In both cases, cancer cells invaded collagen gels to a similar extent as in control conditions (Fig. 1 E), indicating that the physical presence of CAFs in the matrix is necessary to increase cancer cell invasion.

These data show that CAFs induce more cancer cell invasion compared with their paired NAFs and that diffusible molecules of CAFs are not sufficient. Interestingly, the overall ability of fibroblasts to induce cancer cell invasion did not correlate with the expression levels of commonly used CAF markers (Fig. S1 B).

FN deposition by CAFs induces cancer cell invasion

The necessity of CAFs to be physically present in the matrix to induce invasion points toward their role in matrix remodeling. Although NAFs were embedded into the ECM, they did not induce cancer cell invasion. These findings indicate that CAFs, and not NAFs, can remodel the matrix to induce invasion. Proteomic data analysis of two fibroblast couples from colon cancer patients show enrichment in FN in the secretome and proteome of CAFs compared with their paired NAFs (ProteomeXchange Consortium via the PRIDE partner repository with the dataset identifier PXD003670). In addition, FN is known to be enriched in the tumor microenvironment and is a proinvasive ECM protein (Wolanska and Morgan, 2015; Oudin et al., 2016). FN could thus be deposited by CAFs to promote cancer cell invasion. To test this hypothesis, we inhibited FN expression in CAFs using small interfering RNA (Fig. S1 C). Depletion of FN in CAFs from all patients abrogated their ability to stimulate the invasion of cancer cells, indicating that FN is necessary for CAFs to induce cancer cell invasion (Fig. 2 A and Fig. S1 D).

This result was surprising, as it has been shown that CAFs mainly stimulate cancer cell invasion by contracting and aligning the matrix (Gaggioli et al., 2007; Goetz et al., 2011; Calvo et al., 2013). Indeed, live imaging of cancer cell spheroids and CAFs in collagen revealed that CAFs were active in remodeling the matrix (Video 1). CAFs aligned and pulled collagen fibers perpendicularly to the edge of the spheroids, facilitating the migration of cancer cells (Video 2 and Fig. 2, B and C), whereas in the absence of CAFs, collagen fibers were oriented parallel to the spheroid edge (Fig. 2 C), which is not favorable for cancer cell invasion (Provenzano et al., 2006; Kopanska et al., 2016). However, FN-depleted CAFs (CAFsiFN) retained the ability to align collagen fibers in the same fashion (Fig. 2 C). Analysis of the width and length of collagen fibers remodeled by CAFsiCtrl and CAFsiFN also showed no difference between the two cell populations, demonstrating that FN depletion had no effect on the overall topography of the collagen matrix (Fig. 2 D). CAFsiFN also contracted and applied mechanical forces on the matrix similarly to control CAFs, indicating that depletion of FN in CAFs has no consequence on their ability to apply mechanical forces on the matrix (Fig. 2, E and F).

When inhibiting the contractility of CAFs using myosin II inhibitor blebbistatin (Fig. S1 E), collagen alignment and contraction were abrogated, as well as downstream FN assembly, as previously shown (Fig. 2 G; Zaidel-Bar et al., 2007). In this condition, cancer cells did not invade the matrix, either alone or in the presence of CAFs (Fig. S1 F). Together, these results demonstrate that both contractility and FN are important for CAF-mediated cancer cell invasion. However, the overall ability of fibroblasts to induce cancer cell invasion did not significantly correlate with their capacity to contract collagen, especially in the case of couple 3, where NAFs and CAFs displayed similar collagen contraction (Fig. S1 G). This suggests that mechanical forces are important for CAF-mediated cancer cell invasion, as they induce FN assembly. However, if not followed by FN deposition, mechanical forces by CAFs are not sufficient to promote invasion.

Finally, it has been suggested that invadopodia, the actin-rich structures responsible for matrix degradation, could also exert mechanical forces on the matrix and switch on a contractile phenotype (Aung et al., 2014). As contraction and degradation of the matrix could be interdependent, we also checked for the role of proteolysis in CAF-mediated cancer cell invasion. Inhibition of matrix proteolysis using broad spectrum matrix metalloproteinase (MMP) inhibitors GM6001 and

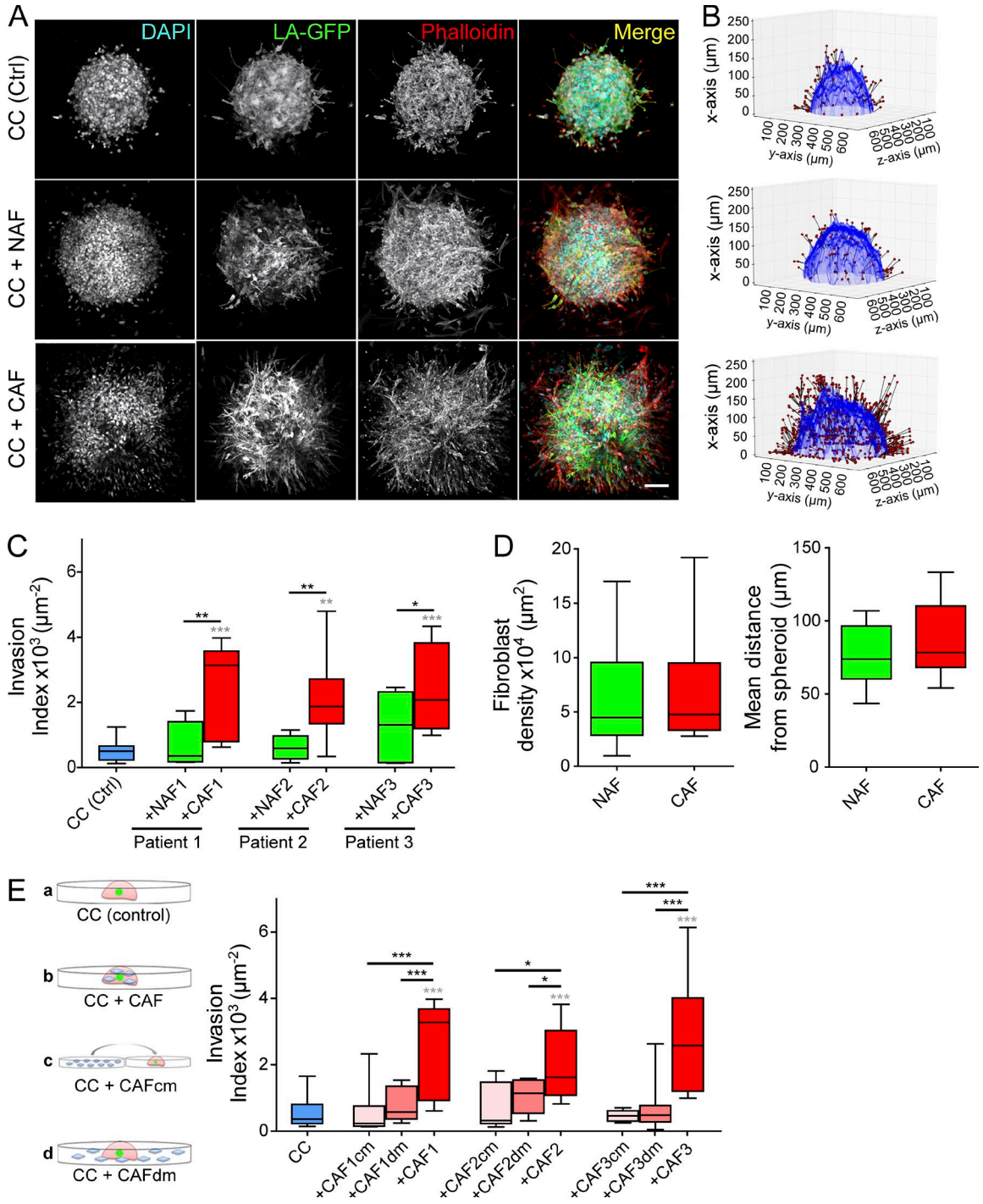

Figure 1. **CAFs induce invasion of cancer cells through matrix remodeling.** (A) Maximum intensity projections of cancer cell spheroids in collagen I, with or without fibroblasts, at day 3. CT26 cancer cells express LifeAct-GFP (green); F-actin (red) and DNA (cyan) were stained with phalloidin-rhodamine and DAPI, respectively. Bar, 100 µm. (B) 3D rendering of spheroids at day 3. Invasion is quantified using the invasion counter software. Red dots represent nuclei of invading GFP cancer cells (migrated out of the spheroid). (C) Quantification of cancer cell invasion alone (blue box) and in the presence of NAFs (green boxes) or CAFs (red boxes) for three different patients. P-values are compared with cancer cells alone (in gray) and to cancer cells with CAFs (in black) using Newman-Keuls multiple comparisons test (*, $P < 0.05$; **, $P < 0.01$; ***, $P < 0.001$). (D, left) Quantification of the density of NAFs and CAFs from all three patients around the spheroid. Fibroblast density is defined as the number of nuclei of non-GFP cells normalized to the surface area of the spheroid contour in 3D. P-value is calculated using Mann–Whitney test. (Right) Quantification of the mean distance of NAFs and CAFs from the spheroid. The mean distance from the spheroid was defined as the distance from the nuclei of non-GFP cells to the closest point along the cancer cell spheroid contour. P-value is calculated using Mann–Whitney test. (E, left) Schematic representation of the experiment. Cancer cells were embedded in collagen gels (a). CAFs were either mixed with cancer cells in the collagen droplet (b), their conditioned media was added to cancer cells (c), or they were plated around the collagen droplet (d). (Right) Quantification of cancer cell invasion alone, in the presence of CAFcm or CAFdm, or in the presence of CAFs for three different patients. Invasion index is defined as the ratio between the number of invading nuclei of GFP cancer cells and the area of the spheroid contour. Quantification results are expressed as box and whiskers (minimum to maximum) of at least $n = 3$ separate experiments. P-values are compared with cancer cells alone (in gray) and to cancer cells with CAFs (in black) using Newman-Keuls multiple comparisons test (*, $P < 0.05$; **, $P < 0.01$; ***, $P < 0.001$). CC, cancer cells.

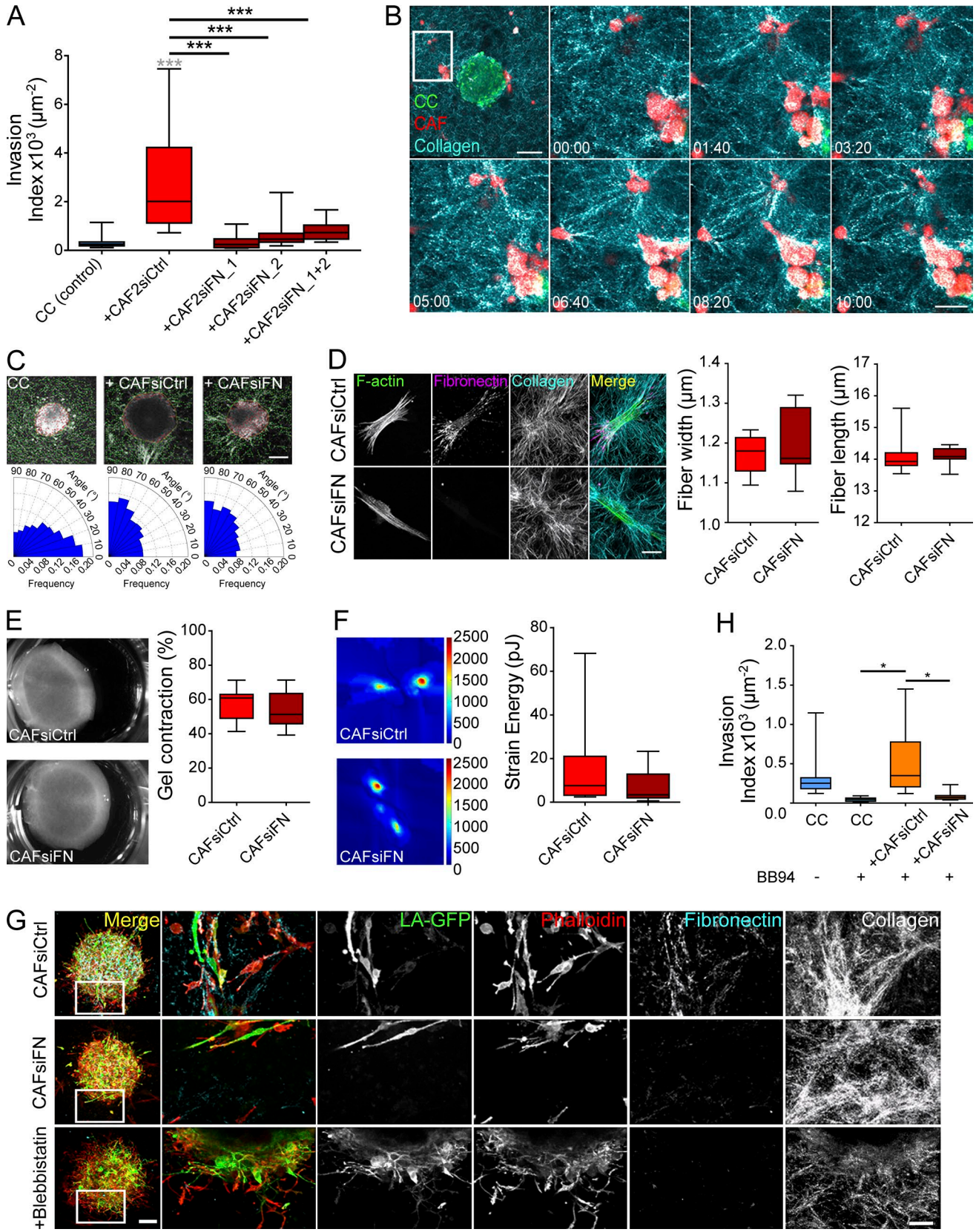

Figure 2. **CAFs deposit FN to induce cancer cell invasion.** (A) Quantification of cancer cell invasion alone or in the presence of CAFs from patient 2, depleted or not for FN. P-values are compared with cancer cells alone (in gray) and to cancer cells with CAFs (in black) using Newman-Keuls multiple comparisons test (***, $P < 0.001$). (B) Time-lapse sequence of CT26 cancer cells and CAFs from patient 1 in collagen. CT26 cancer cells express LifeAct-GFP (green), CAFs are stained with a lyophilic carbocyanine dye (red), and collagen is acquired by reflection (blue). Time is in hours and minutes (HH:mm). Bar, 200 µm. The magnified region is represented by the white square. Bar, 100 µm. (C, top) Overlaid images of collagen I matrices containing cancer

BB94 abrogated the spontaneous invasion of cancer cells, as previously shown (Poincloux et al., 2009; Wolf et al., 2013). Interestingly, CAFs rescued cancer cell invasion in the presence of MMP inhibitors (Fig. S1 H), indicating that CAFs can stimulate an invasion of cancer cells that is independent of MMPs. When treated with BB94, CAFs still contracted collagen plugs; thus, CAFs' ability to contract the matrix did not depend on their ability to degrade it (Fig. S1 I). Interestingly, FN-depleted CAFs failed to rescue cancer cell invasion in the presence of MMP inhibitors (Fig. 2 H and Fig. S1 J).

Together, these data show that in the presence of CAFs that are able to deposit FN, cancer cells can invade the matrix in an MMP-independent manner. These findings could provide an explanation of the failure of MMP inhibitors in clinics. As a major constituent of the tumor microenvironment, CAFs can provide an alternative escape mechanism for cancer cells by aligning collagen fibers and assembling the FN that enables cancer cell invasion.

CAFs secrete and assemble more FN than NAFs

FN fibrillogenesis is a complex multistep process. Cells secrete FN as soluble dimers, which then bind to integrin receptors, unfold, and associate with each other to form a fibrillary matrix (Wolanska and Morgan, 2015). It is possible that CAFs are more efficient in assembling FN than NAFs and consequently induce more invasion of cancer cells. To address this, we compared the capacity of CAFs and NAFs to secrete and assemble FN (Fig. 3, A and B).

The analysis of the conditioned media showed that CAFs secrete more FN compared with NAFs (Fig. 3 A). Similarly, CAFs assembled more FN fibrils compared with their paired NAFs (Fig. 3 B). Moreover, the amounts of secreted and assembled FN by fibroblasts significantly correlated with the invasion index (Fig. 3 C). This result indicates that the ability of fibroblasts to induce cancer cell invasion directly correlates with the amount of FN they produce.

To further discriminate between the roles of secreted and assembled FN in cancer invasion, based on the estimation of the amount of FN secreted by CAFs (Fig. 3 A), we added 250 ng/ml of soluble FN to cancer cell spheroids. We observed that supplementing collagen with soluble FN did not induce invasion (Fig. 3 D). This was not surprising, as CAFs' secreted molecules did not promote cancer cell invasion (Fig. 1 C).

Together, these results show that CAFs secrete and assemble FN more efficiently than NAFs and point toward the importance of FN assembly in CAF-mediated cancer cell invasion. As the invasion induced by all fibroblast populations most significantly correlated with the amount of assembled FN, we uncover a signature of CAFs and a link between ECM remodeling by CAFs and cancer cell invasion. These results are in agreement with a new study in which the analysis of FN expression in tumors from 435 head and neck cancer patients revealed an inverse correlation between high levels of FN and patient prognosis (Gopal et al., 2017). Besides serving as a cue in the ECM that cancer cells haptotact toward (Oudin et al., 2016), FN also establishes chemotactic gradients by modulating the bioavailability of growth factors such as hepatocyte growth factor (Rahman et al., 2005; Hynes, 2009). Therefore, by being in close proximity to each other, CAFs could stimulate the invasion of cancer cells toward FN and the growth factors FN matrices retain.

Integrin-αvβ3 is necessary for FN assembly

As soluble FN did not stimulate cancer cell invasion, we addressed the role of assembled FN. FN is assembled via transmembrane proteins, integrins; more specifically, mostly via integrin-α5β1 and -αvβ3 (Wolanska and Morgan, 2015). We correlated the amounts of integrin isoforms α5, αv, β1, and β3 in CAFs to their ability to induce invasion. Integrin-αv and -β3 expression showed the highest correlation, hinting at the importance of integrin-αvβ3 in CAF-mediated cancer cell invasion (Fig. S2, A and B).

We next tested whether β3- or α5-depleted CAFs (Fig. S2, C and D) could induce invasion. In this condition, the amount of secreted FN by CAFs was unchanged (Fig. S2 E). In the presence of both CAFsi-α5 and CAFsi-β3, invasion was significantly reduced (Fig. 4 A). This effect was confirmed using cilengitide, an inhibitor of integrin-β3 (Fig. 4 B). FN assembly by CAFsi-β3 was markedly reduced compared with control CAFs and α5-depleted CAFs (Fig. 4 C and Fig. S2 F) and was not caused by an impaired migration of CAFs toward cancer cells (Fig. S2 G). These results indicate that integrin-β3 and -α5 are necessary for CAF-mediated cancer cell invasion. They also validate the requirement of FN assembly for cancer cell invasion, as silencing of integrins or blocking of integrin-β3 or of contractility in CAFs does not affect FN secretion but abrogates cancer cell invasion (Fig. S2 E).

Because the fluorescence signal in 3D assays is nontrivial to quantify, we assessed the amount of assembled FN on 2D

cell spheroids alone or together with control or FN-depleted CAFs from patient 1 generated using CurveAlign. The yellow line indicates the edge of the spheroid, and the green lines indicate fiber orientation with respect to the closest point on the spheroid edge. Bar, 100 µm. (Bottom) Rose plots representing the frequency of distribution of the absolute angles of collagen fibers within the range of 0–90° with respect to the closest point on the spheroid edge. (D, left) Maximum intensity projections of CAFs from patient 1 treated with siRNA scrambled control (CAFsiCtrl) or with siRNA targeting FN (CAFsiFN). F-actin is stained with phalloidin-rhodamine (green), FN is immunostained (magenta), and collagen is acquired using second harmonic generation (cyan). Bar, 20 µm. (Right) Quantification of collagen fiber width and length using CT-FIRE. P-value is calculated using Mann–Whitney test for at least $n = 3$ stacks over $n = 2$ separate experiments. (E, left) Control and FN-depleted CAFs from patient 1 cultured in collagen I gels 1 d after embedding. (Right) Percentage of gel contraction of control and FN-depleted CAFs from patient 1 calculated using the formula 100 × [gel area (T0) – gel area(T1)]/gel area (T0). P-value is calculated using Mann–Whitney test for $n = 3$ over $n = 6$ separate experiments. (F, left) Traction force map of control and FN-depleted CAFs from patient 1 on collagen-coated polyacrylamide gels with Young's modulus of 5 kPa. Color code gives the magnitude of traction stress in Pa, which corresponds to forces of piconewton/squared micrometers. (Right) Corresponding mean force (strain energy) exerted by CAFs over a 30-min time lapse. P-value is calculated using Mann–Whitney test for $n = 10$ cells over $n = 2$ separate experiments. (G) Maximum intensity projections of cancer cell spheroids in collagen I gels with CAFs from patient 1 treated with siRNA scrambled control, siRNA against FN, or blebbistatin at day 3. Bar, 100 µm. Magnified regions are represented by the white squares. CT26 cancer cells express LifeAct-GFP (green), F-actin is stained with phalloidin-rhodamine (red), FN is immunostained (cyan), and collagen is acquired using reflection (white). Bar, 50 µm. (H) Quantification of cancer cell invasion alone or in the presence of control or FN-depleted CAFs treated with BB94 from patient 3. Invasion index is defined as the ratio between the number of invading nuclei of GFP cancer cells and the area of the spheroid contour. All quantification results are expressed as box and whiskers (minimum to maximum) of at least $n = 3$ separate experiments. P-values are compared with cancer cells alone (in gray) and to cancer cells with CAFs (in black) using Newman-Keuls multiple comparisons test (*, $P < 0.05$; **, $P < 0.01$; ***, $P < 0.001$).

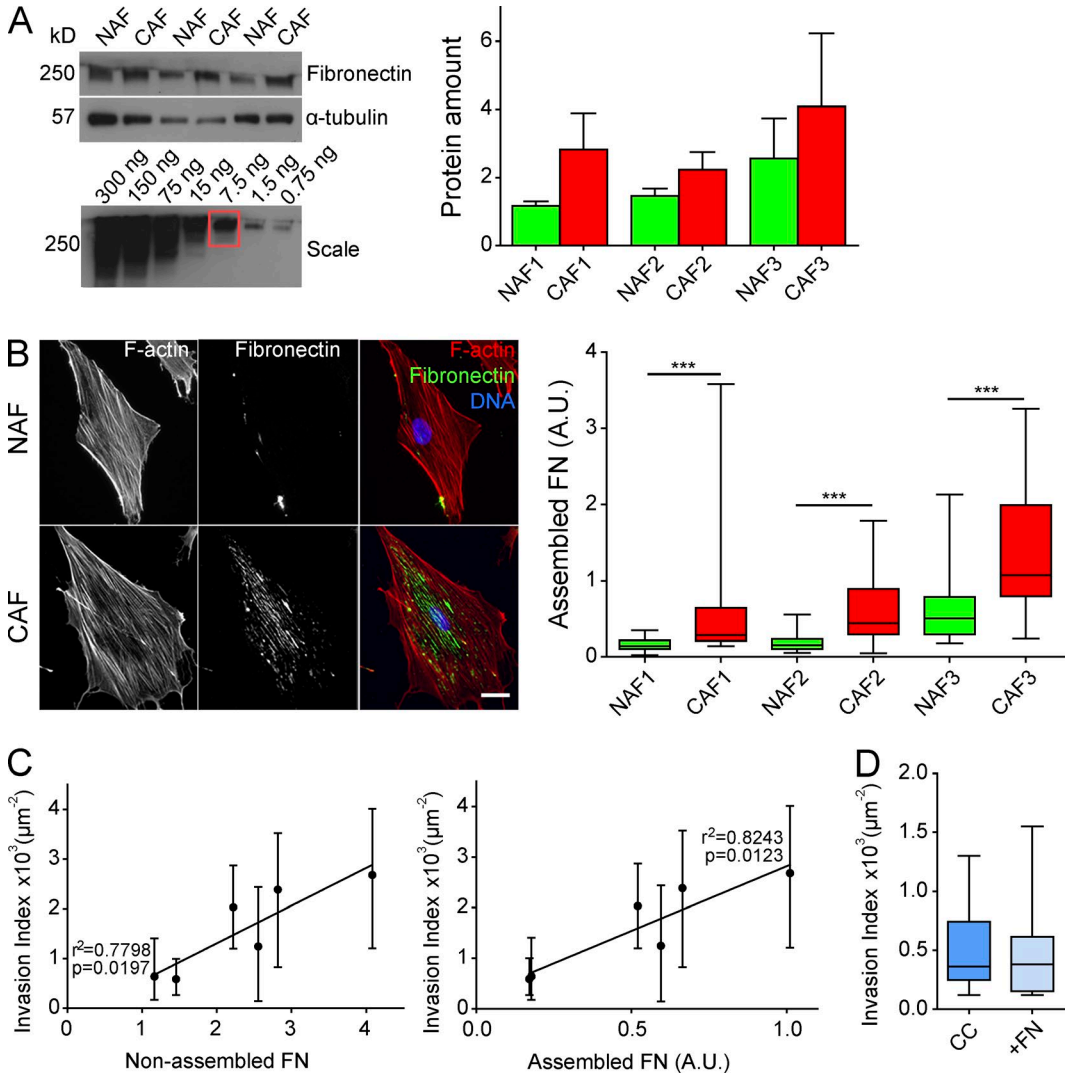

Figure 3. **CAFs secrete and assemble more FN than NAFs.** (A) Immunoblot analysis. Conditioned media prepared from NAFs and CAFs from three patients were probed with FN antibody. α-Tubulin served as a loading control. Protein amount is represented by normalizing to α-tubulin. Results are represented as column bars for $n = 3$ separate experiments. For the FN scale: soluble FN loaded at a range of 300 to 0.75 ng. (B, left) Immunostaining of FN (green) in NAFs and CAFs from three patients. F-actin is stained with phalloidin-rhodamine (red), and DNA was stained with DAPI (blue). Bar, 20 µm. (Right) Quantification of assembled FN. Amount of assembled FN is defined as the amount of fluorescence in a cell (integrated density) normalized to the area of the cell and the background fluorescence. P-value is calculated using Mann–Whitney test for $n = 20$ cells over $n = 2$ separate experiments. (C) Scatter dot graphs correlating the invasion index of cancer cells in the presence of fibroblasts from all three patients with the amount of secreted (left) and assembled FN (right) by fibroblasts. Quality of linear regression is represented by the values of p and r^2. (D) Quantification of cancer cell invasion in a collagen matrix or in a collagen and FN matrix. Invasion index is defined as the ratio between the number of invading nuclei of GFP cancer cells and the area of the spheroid contour. Quantification results are expressed as box and whiskers (minimum to maximum) for at least $n = 3$ separate experiments. ***, $P < 0.001$. A.U., arbitrary units.

substrates. Surprisingly, depletion of integrin-α5 did not alter FN assembly by CAF 1 d after plating, though the ability to assemble FN was reduced upon depletion of integrin-β3 (Fig. S3 A). In contrast, when fibroblasts were cultured for 3 d and allowed to reach confluency, depletion of integrin-α5 or -β3 reduced FN fibrillogenesis (Fig. 4 D). These results suggest that integrin-β3 mediates FN assembly at an early stage, whereas α5 could be required later on for sustained assembly of FN fibers.

Integrin-α5 and -β3 are required at different stages of FN fibrillogenesis

As our results indicate that both integrin-α5β1 and -αvβ3 are required for FN fibrillogenesis, we next wondered about their localization in CAFs and with respect to FN fibers. In 2D, integrin-α5 was found in the center of the cells in mature fibrillar adhesions colocalizing with FN fibers. αvβ3 was present at the cell periphery, at focal adhesions partially colocalizing with FN puncta (Fig. 5 A). In 3D collagen matrices, integrin-αvβ3 accumulated at the cell poles along with FN deposits (Fig. 5 B), whereas integrin-α5 was localized all along the cell periphery (Fig. S3 B).

The localization of integrin-αvβ3 at the cell periphery suggests its requirement during initial cell–matrix interactions. Indeed, after letting the cells adhere for 2 h, integrin-αvβ3 already clustered, whereas integrin-α5 was not yet recruited (Fig. 5 C). However, as blocking of integrin-β3 did not alter the CAFs' contractility (Fig. S3 C), these results indicate that integrin-αvβ3 is required at the initial steps of FN fibrillogenesis, downstream of contractility.

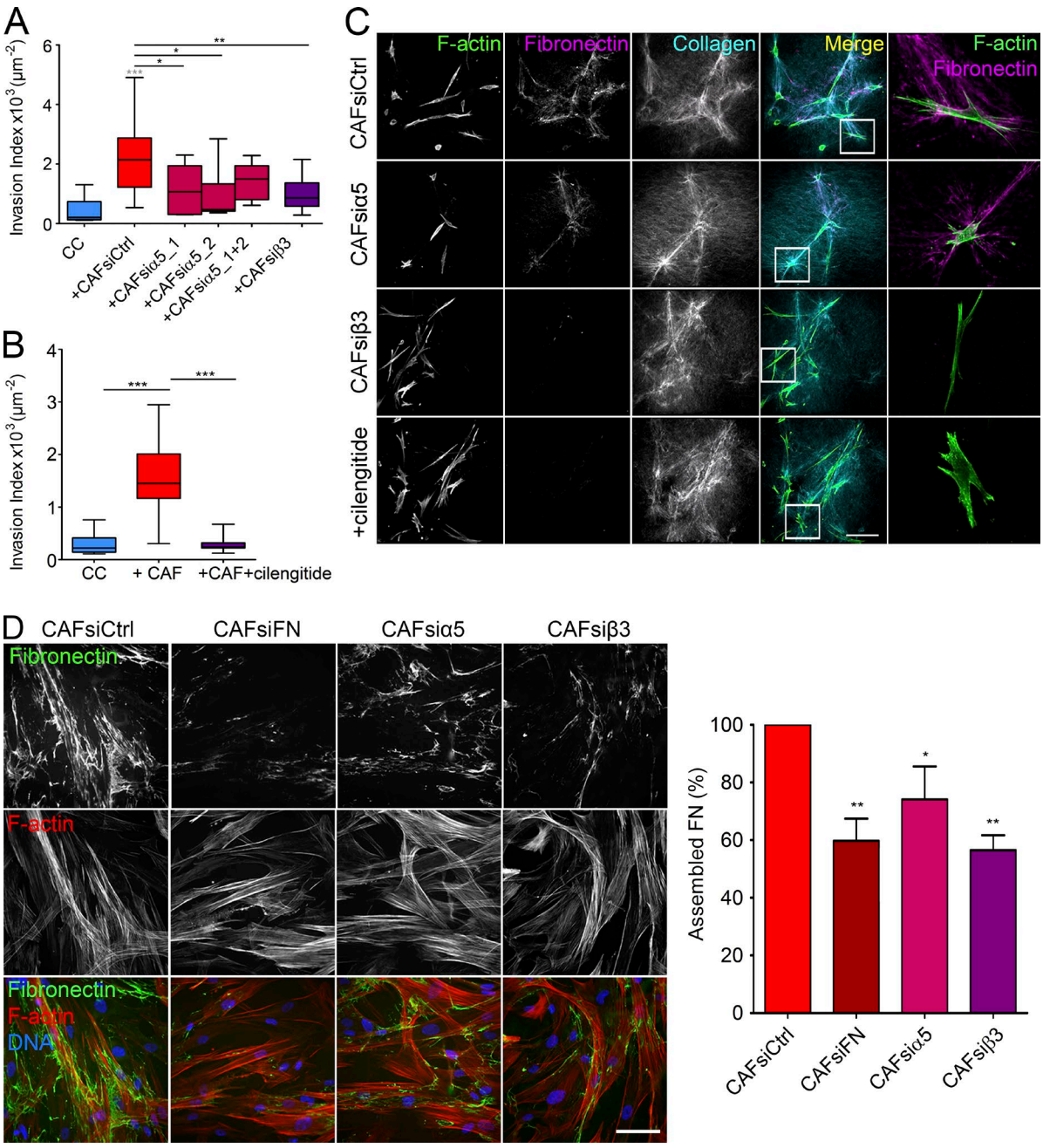

Figure 4. **Integrin-αvβ3 is necessary for FN assembly.** (A) Quantification of cancer cell invasion alone or in the presence of control CAFs, α5-depleted CAFs, and β3-depleted CAFs from patient 3. (B) Quantification of cancer cell invasion in the presence of CAFs from patient 2, with or without cilengitide treatment. (A and B) Invasion index is defined as the ratio between the number of invading nuclei of GFP cancer cells and the area of the spheroid contour. All quantification results are expressed as box and whiskers (minimum to maximum) of at least $n = 3$ separate experiments. P-values are compared with cancer cells alone (in gray) and to cancer cells with CAFs (in black) using Newman-Keuls multiple comparisons test (*, $P < 0.05$; **, $P < 0.01$; ***, $P < 0.001$). (C) Maximum intensity projections of CAFs from patient 2 treated with siRNA scrambled control, siRNA against integrin-α5 or integrin-β3, or cilengitide. Bar, 100 µm. Magnified regions are represented by the white squares. F-actin is stained with phalloidin-rhodamine (green), FN is immunostained (magenta), and collagen is acquired using second harmonic generation (cyan). Bar, 20 µm. (D, left) Immunostaining of FN (green) in control CAFs, FN-depleted CAFs, α5-depleted CAFs, and β3-depleted CAFs from patient 2, 3 d after plating. F-actin was stained with phalloidin-rhodamine (red), and DNA was stained with DAPI (blue). Bar, 40 µm. (Right) Graph represents the percentage of assembled FN relative to control conditions defined as the amount of fluorescence in a monolayer (integrated density) normalized to the number of nuclei. Quantification results are expressed as column bars with mean ± SEM. Depleted CAFs were compared with control CAFs for $n = 10$ frames over $n = 4$ separate experiments. P-value is calculated using Newman Keuls multiple comparisons test (*, $P < 0.05$; **, $P < 0.01$; ***, $P < 0.001$).

Integrin-β3 specifically accumulates at areas of high-traction force and is stationary within focal adhesions, whereas integrin-β1 is more mobile and thus prone to relocate to fibrillar adhesions (Rossier et al., 2012; Schiller et al., 2013). Inhibition of myosin disassembles β3 clusters without affecting levels and localization of integrin-β1 (Schiller et al., 2013). This could explain why treatment of CAFs with blebbistatin abrogates FN assembly. However, depletion of αvβ3 does not alter CAFs' ability to contract collagen, indicating that αvβ3 is downstream of contractility.

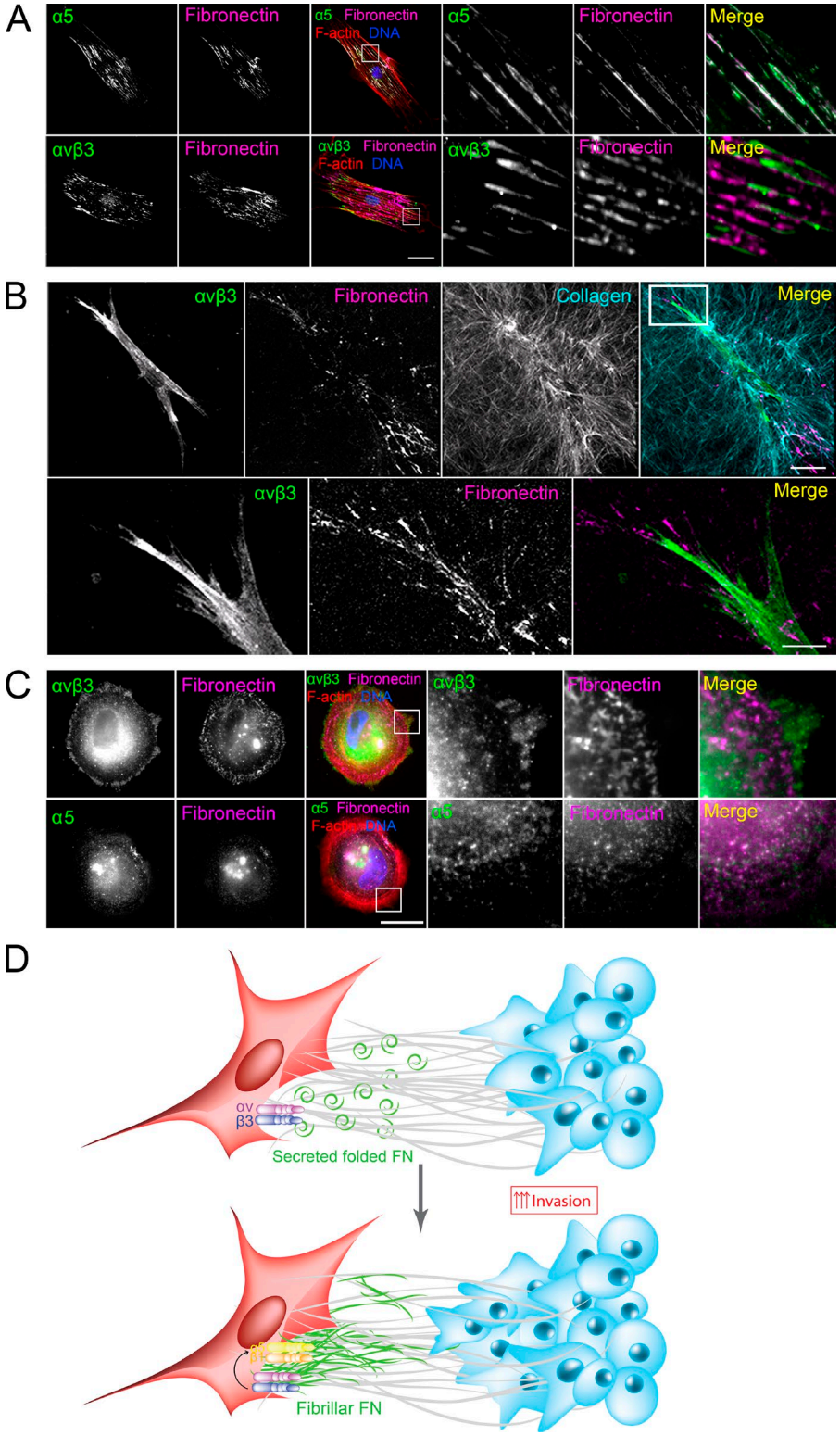

Figure 5. **Integrin-α5 and -β3 are required at different stages of FN fibrillogenesis.** (A) Immunostaining of CAFs on 2D coverslips for integrins α5 and αvβ3 (green) and FN (magenta). F-actin was stained with phalloidin-rhodamine (red), and DNA was stained with DAPI (blue). Bar, 40 µm. (B) Maximum intensity projections of CAFs in 3D collagen matrices immunostained for integrin-αvβ3 (green) and FN (magenta). Collagen was acquired using second harmonic generation (cyan). Bars: (main image) 40 µm; (magnified image) 10 µm. (C) Immunostaining of CAFs 2 h after plating for integrin-α5 or -αvβ3 (green) and FN (magenta). F-actin was stained with phalloidin-rhodamine (red), and DNA was stained with DAPI (blue). Bar, 20 µm. (A–C) Magnified regions are represented by white squares. (D) Model: CAFs present in the collagen I–rich tumor stroma secrete FN. (Top) Contractile forces exerted by CAFs align the ECM and activate αvβ3 at the sites of focal adhesions. (Bottom) αvβ3 activation leads to the formation of fibrillar adhesions and FN fibrillogenesis.

In cells plated on RGD-rich substrates, αvβ3 localizes at focal adhesions and, unlike β1, is responsible for force-dependent focal adhesion maturation (von Wichert et al., 2003; Roca-Cusachs et al., 2013; Changede et al., 2015). Thus, αvβ3 could be involved in mediating the signal, from contractility to formation of fibrillar adhesions. This hypothesis is supported by a study showing that pulling on vascular smooth muscle cells using anti-β3 antibody–coated beads, and not α2 or β1, resulted in the activation of downstream signaling (Goldschmidt et al., 2001). Similarly, a blockade of integrin-β3, but not -β1, abrogates DNA synthesis induced by mechanical strain in vascular smooth muscle cells (Wilson et al., 1995).

Because in our study we used collagen, which is not an RGD substrate, αvβ3 localization at focal adhesions is

somewhat surprising. The possible explanation is that because of the presence of serum and cellular FN secreted by the cells themselves, cells are constantly exposed to RGD motifs. It has also been shown that αvβ3 localizes to the cell's edge independently of RGD upon stimulation by growth factors such as FGF (Kiosses et al., 2001). In the context of a tumor where CAFs, blood vessels, or cancer cells constantly secrete FN and growth factors, the nature of the matrix would not really matter, as it is constantly enriched in RGD peptides.

In conclusion, our study shows that diffusible molecules secreted by CAFs are not sufficient to induce cancer cell invasion. Instead, CAFs' remodeling of the matrix is the key player. We propose a model in which contractility of CAFs is necessary for downstream activation of the integrin-αvβ3 and assembly of FN puncta. α5β1 becomes critical only at later stages of FN assembly at fibrillar adhesions (Fig. 5 C). Because the ability of all fibroblast populations to assemble FN directly correlates with their ability to induce cancer cell invasion, we demonstrate that ECM deposition (more specifically, FN fibrillogenesis) is the key component for CAF-mediated cancer cell invasion. Finally, we show that integrin-β3 is the major driver for FN assembly in CAFs, as its inhibition abrogates CAF-mediated cancer cell invasion.

Materials and methods

Cell lines

CT26 mouse intestinal cancer cells were obtained from American Type Culture Collection. Cells were cultured in DMEM (Life Technologies) supplemented with 10% FBS (Invitrogen) and 5% CO_2. Cells were infected with a lentiviral GFP plasmid according to standard procedures.

Isolation and culture of primary fibroblasts

Human primary fibroblasts were isolated from fresh colon tumors (CAFs) and adjacent noncarcinoma tissue (NAFs) samples from patients treated at Lariboisière Hospital, Paris, with the written consent of the patients and approval of the local ethics committee. Samples were treated as previously described (Amatangelo et al., 2005). In brief, tissues were collected after surgical resection in RPMI buffer and washed in PBS supplemented with 10% antibiotic–antimycotic (AA; Gibco). 100-mm^2 tissue culture plates were scratched using a scalpel, and tissue pieces of ∼1–2 mm^2 were cut and placed on the junctions. After isolation, the tumor pieces were kept in 10 ml DMEM supplemented with 10% FBS (Life Technologies) and 10% AA. 24 h later, the medium was changed and AA concentration was reduced to 5%. From this point, the medium was changed every 2 d, reducing AA concentration by half every time, until AA concentration reached 1%. Fibroblasts typically started going out of the tissues after 2–3 wk. When having reached confluency, fibroblasts were trypsinized and plated on 30 KPa of 30-mm^2 soft plates (Excellness) that were previously coated with 5 µg/ml of rat tail collagen I (Corning) in DMEM polymerized at 37°C for at least 24 h. Soft plates were used to avoid activation of fibroblasts by matrix rigidity. Unless stated otherwise, all fibroblasts were cultured on soft plates and kept in their primary nontransformed state until passage 10. After isolation, all cell populations were characterized for the presence of markers of activated fibroblasts: α-SMA, FAP, and PDGFR-β (Fig. S1 A).

Western blotting

Protein lysates were obtained from fibroblasts seeded on soft plates at passage 3. Protein lysates were processed according to standard procedures. In brief, cells were washed with PBS, lysed in radioimmunoprecipitation assay buffer (1% Triton X-100, 50 mM Tris, pH 7.5, 1 mM EDTA, and 150 mM NaCl) supplemented with protease and phosphatase inhibitor cocktails (Sigma-Aldrich), and boiled in Laemmli buffer for 5 min. The samples were separated in SDS-PAGE gradient gels (4–15%), transferred to a nitrocellulose membrane using the BioRad system, and blocked in 5% nonfat dried milk dissolved in PBS supplemented with 0.1% Tween for 30 min at RT. The membranes were incubated with primary antibodies overnight at 4°C followed by incubation with peroxidase-conjugated secondary antibodies for 1 h at RT. Immunoreactive bands were detected using an ECL-plus kit (Roche). Quantifications were done using ImageJ (National Institutes of Health) by normalizing the protein amount to α-tubulin or GAPDH amounts (loading controls). Antibody description and working dilutions can be found in Table S1.

Invasion assay

Agarose (Invitrogen) was dissolved in water to a concentration of 0.01 g/ml and boiled. 150 µl of the solution was added to a 48-well plate, and agarose was left to polymerize for at least 10 min at RT. A solution of 10^4 cells/ml of CT26 cancer cells was made, and 75–100 µl of the solution was added to the wells. The wells were subsequently filled with DMEM supplemented with 10% FBS, and spheroids were left to form for 3–4 d.

30-mm^2 tissue culture plates were specifically fashioned for the invasion assay: three holes ∼3–4 mm in diameter were drilled in a plate and widened around the edges using a scalpel. The bottom of the dish was covered with epoxy (Loctite), and 20 × 20–mm square coverslips were glued to the dish overnight at RT. 1 d before the experiment, the dishes were silanized with 3-aminopropyl-trimethoxysilane (Sigma-Aldrich). The dishes were washed extensively with water and treated for 30 min with 0.5% glutaraldehyde followed by a final wash. This treatment was made to avoid collagen detachment from the plastic holes because of the high contractility exerted by CAFs.

2 mg/ml of rat tail collagen I (Corning) was prepared in DMEM, 10× PBS, and 1 M NaOH, to a pH of 7. The solution was kept on ice to avoid collagen polymerization. Spheroids were embedded in 15 µl collagen drops containing 5 × 10^3 fibroblasts, positioned in the hole of the culture plate. After filling all three holes, the plate was flipped every 30 s for 5 min in order for the cells to stay in the middle of the collagen drop (preventing sedimentation of spheroids to the glass or to the collagen/air interface). Collagen was left to polymerize for an additional 15 min at RT before 3 ml DMEM supplemented with 5% FBS and 1% AA were added. Cancer cells were left to invade for 3 d before fixing and staining.

For evaluation of cancer cell invasion in the presence of CAFdm, 15 × 10^3 CAFs were plated around the three collagen droplets on the plastic dish. For evaluation of cancer cell invasion in the presence of CAFcm, three sets of 15 × 10^3 CAFs were plated on 30-mm^2 soft plates in DMEM supplemented with 10% FBS for 1 d to properly adhere. CAFs were then extensively washed with serum-deprived DMEM and incubated in 1 ml of serum-deprived media. Conditioned media were harvested 24 h later (3 ml in total), supplemented with 5% FBS and 1% AA, and added on a tissue culture plate containing three collagen droplets of single spheroids.

Collagen contraction assay

1.5 × 10^5 fibroblasts were suspended in 1.5 ml of 2-mg/ml rat tail collagen I (Corning) and added to a 24-well plate in triplicates (500 µl/well). After 30 min of incubation at RT, collagen plugs were detached from the walls of the well with a scalpel, and DMEM supplemented with 10% FBS was added. Images of the collagen plugs were acquired

at time 0 (T0) and after 24 h (T1) using a microscope (M165FC; Leica). To obtain the gel contraction value, the relative area of the gel was measured using ImageJ software at T0 and T1, and the percentage of contraction was calculated using the formula $100 \times [\text{gel area (T0)} - \text{gel area (T1)}]/\text{gel area (}T0\text{)}$.

Collagen topography measurements

Fibers' alignment and their angles with respect to the spheroid edge were measured on images acquired using reflection microscopy with the available software, CurveAlign in MatLab. The angles of collagen fibers compared with the spheroid edge were determined for 10 slices per condition. Fiber width and length were measured on images acquired using second harmonic generation with the available software, CT-FIRE in MatLab.

Inhibitors and siRNA

Blebbistatin (Sigma-Aldrich), BB94 (AbCam), and cilengitide (Selleckchem) were used at 15, 5, and 1 µM, respectively. They were mixed with the media and added to the invasion assay after collagen polymerization. GM6001 (Millipore) was used at 20 µM and was mixed with both the collagen before its polymerization and added to the media as previously described (Wolf et al., 2013).

For protein knockdowns using siRNA, CAFs were cultured in standard conditions and transfected using HiPerFect (301704; Qiagen). 6×10^4 CAFs were plated in a well of a 6-well plate and subjected to transfection using 100 nM siRNA. siRNA was purchased from Qiagen, and sequences are listed in Table S2.

3D immunofluorescence

Spheroids embedded in collagen were fixed using 4% PFA in PBS for 30 min at RT and washed with PBS. Anti-FN antibody was added in 500 µl PBS, and dishes were left under agitation at RT for 2 d. Spheroids were then washed with PBS and permeabilized with 0.1% Triton X-100 in PBS for 30 min at RT. DNA and F-actin were stained using DAPI and phalloidin, respectively (Life Technologies). Collagen was imaged using confocal reflection microscopy.

For integrin stainings, CAFs were embedded in collagen drops for 3 d in identical culture conditions and then fixed and stained similarly to spheroids. Permeabilization was performed for 15 min to avoid damaging the cell membrane. Antiintegrin antibodies were added in 500 µl PBS, and the dishes were left under agitation at RT for 2 d. Appropriate secondary antibodies were added in 500 µl PBS along with phalloidin-rhodamine. Collagen was imaged using second harmonic generation. In all conditions, cells were imaged at a similar distance from the coverslip using the same settings.

Quantification of FN secretion and expression

CT26 cancer cells were incubated in 10 ml of serum-deprived DMEM at a density of 10^6 cells for 24 h. The media were collected, passed through 0.2-µm filters to eliminate cell debris, and added on soft plates containing 1.5×10^5 fibroblasts for 3 d. The media were collected, filtered again, and a 300-µl sample was processed according to Western blot standard procedures. 30 µl of all samples was loaded into a polyacrylamide SDS-PAGE gel (our Laemmli sample buffer being 2× concentrated, this volume corresponds to 15 µl of sample). For the purified FN scale, samples were loaded in the same fashion with an FN concentration ranging from 50 ng/ml to 20 µg/ml (corresponding total FN amount ranging from 0.75 to 300 ng).

For quantification of FN secretion by integrin and FN-depleted CAFs, CAFs were plated in a well of a 6-well plate and treated with RNAi against FN as previously described in the section Inhibitors and siRNA. CAFs were then extensively washed with serum-free DMEM, incubated in 1 ml of serum-free DMEM, and retransfected with another round of siRNA to maintain protein depletion. Media were collected, filtered, and processed for Western blotting as already described.

Cytotoxicity and viability tests

10^4 CAFs were plated in triplicate in a 96-well plate in DMEM supplemented with 10% FBS and treated with siRNA for 3 d as described in the Inhibitors and siRNA section. For testing cilengitide effects, CAFs were plated in the same conditions for 3 d without siRNA treatment. CAFs were then washed and treated with either another round of siRNA or 1 µM cilengitide for 24 h. 100 µl of conditioned media of each condition was harvested for cytotoxicity tests using the Cytotoxicity Detection kit LDH (Roche) according to the manufacturer's recommendations. Remaining cells were used for viability tests using cell proliferation reagent WST-1 (Roche) according to the manufacturer's recommendations.

2D immunofluorescence

For quantification of FN assembly in CAFs and NAFs, fibroblasts were plated on glass coverslips in CT26-conditioned media. For the remaining 2D stainings, fibroblasts were plated on glass coverslips in DMEM supplemented with 10% FBS. For staining of early FN assembly and integrin localization, cells were fixed 24 h after plating. For staining of mature FN fibers on confluent monolayers, cells were fixed 3 d after plating. Cells were fixed using 4% PFA in PBS for 20 min at RT and washed with PBS. Anti-FN antibody was added for 1 h at RT. Cells were then washed and permeabilized with 0.1% Triton X-100 in PBS for 5 min at RT. Antiintegrin antibodies were added for 1 h at RT. After an additional round of PBS washing, secondary antibodies along with DAPI and phalloidin were added for 1 h at RT to stain DNA and F-actin, respectively. Coverslips were mounted on slides in AquaPolymount (Polysciences) and imaged using an upright wide-field microscope (DM6000; Leica) with a 63×/1.32 NA oil immersion objective. The images were processed and quantified with ImageJ. The amount of assembled FN per cell is calculated by normalizing the amount of fluorescence in a cell (integrated density) to the area of the cell and the background fluorescence.

Traction force microscopy

Traction force microscopy experiments were performed as previously described (Elkhatib et al., 2014). For traction force measurements, FluoSphere bead solution (0.2 µm, 505–515 nm; Invitrogen) was added at 2.5% volume. For time-lapse imaging, we used an inverted wide confocal spinning-disk microscope (40× oil immersion objective, NA 1.3; Roper/Nikon). A fluorescent image of beads and a phase contrast image of the cells were recorded every 3 min during 30 min. At the end of the measurement, cells were detached by adding 10% Triton X-100 (Euromedex), and a reference image without cells was recorded. To ensure good quality imaging of fluorescent beads, we performed Z stacks of 30 images with a distance of 1 µm and automatically chose the optimal focus (MetaMorph software). We used a previously described correlation algorithm to extract the bead displacement fields (Elkhatib et al., 2014).

Imaging 3D samples

For time-lapse experiments, CAFs were stained with a lyophilic carbocyanine dye (Vybrant DiI-Cell Labeling Solutions; ThermoFisher) according to the manufacturer's recommendation. Cells were embedded in collagen as described in the Invasion assay section. The dish was incubated at 5% CO_2 and 37°C in the on-stage incubator (Okolab). For fixed and live 3D samples, images were acquired with an inverted AOBS two-photon laser-scanning confocal microscope (SP8; Leica) coupled with a femtosecond laser (Chameleon Vision II; Coherent Inc.)

using a 25×/1.0 NA water immersion objective. The microscope was equipped with three nondescanned HyD detectors: NDD1 (500–550 nm), NDD2 (≥590 nm), and NDD3 (405 nm). Fluorescence channels were recorded simultaneously using the excitation wavelength 980 nm. Collagen was visualized by either second harmonic generation using the excitation wavelength 910 nm or by confocal reflectance microscopy that does not interfere with DAPI staining, using light at a wavelength of 488 nm and a standard photomultiplier tube detector at a low gain (500 V). Images were recorded every 10 min up to 72 h. 3D stacks were obtained at a step size of 2-µm intervals. The images were processed with the Leica Application Suite, ImageJ, and Imaris (Bitplane).

Invasion counter software

Quantification of cell invasion from spheroids was performed using a custom semiautomated image analysis program written in Python using the following packages: numpy, scipy, matplotlib, scikit-image, and PyQt4. Image stacks of nuclei were first loaded into a custom GUI, and the spheroid contour was determined using adjustable Gaussian filtering, thresholding, and 3D morphological operations. The nuclei of invading cells were then automatically detected using adjustable Gaussian filtering, thresholding, and size exclusion. Centroid positions were determined by taking a weighted mean of the intensity for each nucleus. The positions of invading cancer cell nuclei were then manually verified and modified as necessary. Based on the LifeAct-GFP signal (expressed in cancer cells only), the nuclei of cancer cells were discriminated from the nuclei of fibroblasts. The invasion index, defined as the number of invading cancer cells normalized to the surface area of the spheroid contour in 3D, was then determined. This normalization is necessary to control for the slight variability in spheroid size. Because of the high optical density of the spheroids, only the bottom half of the spheroid was visible. To quantify the distance of fibroblasts from the spheroid, the distance from the nuclei of non–LifeAct-GFP cells to the closest point along the cancer cell spheroid contour was determined. Fibroblast density was defined as the number of nuclei of non-GFP cells normalized to the surface area of the spheroid contour in 3D.

Statistical analyses

All experiments were performed in triplicates in two to six independent experiments. All statistical analysis and graphic representations were performed using Prism software (GraphPad). Data are represented as box and whiskers (minimum to maximum). To show protein amounts and percentages, data are represented as column bars (mean ± SEM). Statistical significance was determined with one-way ANOVA. The Newman-Keuls test was applied for multiple comparisons of different conditions. The Mann–Whitney *t* test was applied for paired comparisons.

Online supplemental material

Fig. S1 shows (a) the levels of CAF markers in all fibroblast populations, (b) the effect of FN depletion on cancer cell invasion in CAFs from all couples, (c) that blocking of contractility inhibits cancer cell invasion but that contractility of fibroblasts does not correlate with invasion, and (d) the effect of MMP inhibition on cancer cell invasion. Fig. S2 shows the levels of integrins in all fibroblast populations and the effects of integrin-α5 and -β3 depletion on fibroblast viability, migration, FN secretion, and cancer cell invasion. Fig. S3 shows that depletion of integrin-β3 inhibits FN assembly in CAFs 24 h after plating, but not contractility and integrin-α5 localization in CAFs embedded in collagen. Videos 1 and 2 show live imaging of cancer cell spheroids and CAFs embedded in collagen. Tables S1 and S2 list antibodies and siRNA sequences, respectively, used in this study.

Acknowledgments

We thank all the members of the Vignjevic laboratory for helpful discussions and for proofreading the manuscript, especially Ralitza Staneva and Shruthi Narayanan for explanations on the CurveAlign software. We especially thank Marie Irondelle, Matthieu Maurin, and Olivier Renaud for their help with high-resolution imaging of integrin stainings.

We acknowledge the Nikon Imaging Center at Centre National de la Recherche Scientifique-Institut Curie, PICT-IBiSA at Lhomond, supported by the Fondation pour la Recherche Médicale (grant FRM N° DGE20111123020), the Cancérôple-IdF (grant n°2012-2-EML-04-IC-1), the National Cancer Institute (grant n° 2011-1-LABEL-IC-4), the Cell and Tissue Imaging Platform - PICT-IBiSA (member of France–Bioimaging, ANR-10-INBS-04) of the Genetics and Developmental Biology Department (UMR3215/U934) of Institut Curie for help with light microscopy, supported by the Agence Nationale de la Recherche (grant ANR-11 BSV2 012 01), the European Research Council (grant F. DEL BENE, ERC ZEBRATECTUM N°311159), and the Fondation pour la Recherche sur le Cancer (ARC SFI20121205686). We also thank La Ligue Contre le Cancer (grant to Y. Attieh) and the European Molecular Biology Organization (grant to A.G. Clark). This work was supported by Labex CelTisBioPhy (grant to Y. Attieh and D.M. Vignjevic) and ERC-2012-StG_20111109 grant STARLIN (to D.M. Vignjevic).

The authors declare no competing financial interests.

Author contributions: Y. Attieh and D.M. Vignjevic conceived of the study. Y. Attieh performed the majority of the experiments. C. Grass helped with experiments. N. Elkhatib and T. Betz assisted with traction force microscopy. A.G. Clark wrote the program to quantify cell invasion. P. Mariani, M. Pocard, and S. Richon collected clinical samples for the study. B. Gurchenkov assisted with live experiments. Y. Attieh and D.M. Vignjevic wrote the manuscript with input from A.G. Clark. D.M. Vignjevic supervised the project.

Submitted: 6 February 2017
Revised: 6 July 2017
Accepted: 1 August 2017

References

Amatangelo, M.D., D.E. Bassi, A.J. Klein-Szanto, and E. Cukierman. 2005. Stroma-derived three-dimensional matrices are necessary and sufficient to promote desmoplastic differentiation of normal fibroblasts. *Am. J. Pathol.* 167:475–488. http://dx.doi.org/10.1016/S0002-9440(10)62991-4

Attieh, Y., and D.M. Vignjevic. 2016. The hallmarks of CAFs in cancer invasion. *Eur. J. Cell Biol.* 95:493–502. http://dx.doi.org/10.1016/j.ejcb.2016.07.004

Aung, A., Y.N. Seo, S. Lu, Y. Wang, C. Jamora, J.C. del Álamo, and S. Varghese. 2014. 3D traction stresses activate protease-dependent invasion of cancer cells. *Biophys. J.* 107:2528–2537. http://dx.doi.org/10.1016/j.bpj.2014.07.078

Calvo, F., N. Ege, A. Grande-Garcia, S. Hooper, R.P. Jenkins, S.I. Chaudhry, K. Harrington, P. Williamson, E. Moeendarbary, G. Charras, and E. Sahai. 2013. Mechanotransduction and YAP-dependent matrix remodelling is required for the generation and maintenance of cancer-associated fibroblasts. *Nat. Cell Biol.* 15:637–646. http://dx.doi.org/10.1038/ncb2756

Changede, R., X. Xu, F. Margadant, and M.P. Sheetz. 2015. Nascent Integrin Adhesions Form on All Matrix Rigidities after Integrin Activation. *Dev. Cell.* 35:614–621. http://dx.doi.org/10.1016/j.devcel.2015.11.001

De Wever, O., Q.D. Nguyen, L. Van Hoorde, M. Bracke, E. Bruyneel, C. Gespach, and M. Mareel. 2004. Tenascin-C and SF/HGF produced by myofibroblasts in vitro provide convergent pro-invasive signals to human colon cancer cells through RhoA and Rac. *FASEB J.* 18:1016–1018.

Elkhatib, N., M.B. Neu, C. Zensen, K.M. Schmoller, D. Louvard, A.R. Bausch, T. Betz, and D.M. Vignjevic. 2014. Fascin plays a role in stress fiber

organization and focal adhesion disassembly. *Curr. Biol.* 24:1492–1499. http://dx.doi.org/10.1016/j.cub.2014.05.023

Gaggioli, C., S. Hooper, C. Hidalgo-Carcedo, R. Grosse, J.F. Marshall, K. Harrington, and E. Sahai. 2007. Fibroblast-led collective invasion of carcinoma cells with differing roles for RhoGTPases in leading and following cells. *Nat. Cell Biol.* 9:1392–1400. http://dx.doi.org/10.1038/ncb1658

Geraldo, S., A. Simon, and D.M. Vignjevic. 2013. Revealing the cytoskeletal organization of invasive cancer cells in 3D. *J. Vis. Exp.* 80:e50763.

Goetz, J.G., S. Minguet, I. Navarro-Lérida, J.J. Lazcano, R. Samaniego, E. Calvo, M. Tello, T. Osteso-Ibáñez, T. Pellinen, A. Echarri, et al. 2011. Biomechanical remodeling of the microenvironment by stromal caveolin-1 favors tumor invasion and metastasis. *Cell.* 146:148–163. http://dx.doi.org/10.1016/j.cell.2011.05.040

Goldschmidt, M.E., K.J. McLeod, and W.R. Taylor. 2001. Integrin-mediated mechanotransduction in vascular smooth muscle cells: frequency and force response characteristics. *Circ. Res.* 88:674–680. http://dx.doi.org/10.1161/hh0701.089749

Gopal, S., L. Veracini, D. Grall, C. Butori, S. Schaub, S. Audebert, L. Camoin, E. Baudelet, A. Radwanska, S. Beghelli-de la Forest Divonne, et al. 2017. Fibronectin-guided migration of carcinoma collectives. *Nat. Commun.* 8:14105. http://dx.doi.org/10.1038/ncomms14105

Hynes, R.O. 2009. The extracellular matrix: not just pretty fibrils. *Science.* 326:1216–1219. http://dx.doi.org/10.1126/science.1176009

Joyce, J.A., and J.W. Pollard. 2009. Microenvironmental regulation of metastasis. *Nat. Rev. Cancer.* 9:239–252. http://dx.doi.org/10.1038/nrc2618

Kalluri, R. 2016. The biology and function of fibroblasts in cancer. *Nat. Rev. Cancer.* 16:582–598. http://dx.doi.org/10.1038/nrc.2016.73

Kalluri, R., and M. Zeisberg. 2006. Fibroblasts in cancer. *Nat. Rev. Cancer.* 6:392–401. http://dx.doi.org/10.1038/nrc1877

Kiosses, W.B., S.J. Shattil, N. Pampori, and M.A. Schwartz. 2001. Rac recruits high-affinity integrin alphavbeta3 to lamellipodia in endothelial cell migration. *Nat. Cell Biol.* 3:316–320. http://dx.doi.org/10.1038/35060120

Kopanska, K.S., Y. Alcheikh, R. Staneva, D. Vignjevic, and T. Betz. 2016. Tensile Forces Originating from Cancer Spheroids Facilitate Tumor Invasion. *PLoS One.* 11:e0156442. http://dx.doi.org/10.1371/journal.pone.0156442

Labernadie, A., T. Kato, A. Brugués, X. Serra-Picamal, S. Derzsi, E. Arwert, A. Weston, V. González-Tarragó, A. Elosegui-Artola, L. Albertazzi, et al. 2017. A mechanically active heterotypic E-cadherin/N-cadherin adhesion enables fibroblasts to drive cancer cell invasion. *Nat. Cell Biol.* 19:224–237. http://dx.doi.org/10.1038/ncb3478

Mueller, M.M., and N.E. Fusenig. 2004. Friends or foes - bipolar effects of the tumour stroma in cancer. *Nat. Rev. Cancer.* 4:839–849. http://dx.doi.org/10.1038/nrc1477

Orimo, A., P.B. Gupta, D.C. Sgroi, F. Arenzana-Seisdedos, T. Delaunay, R. Naeem, V.J. Carey, A.L. Richardson, and R.A. Weinberg. 2005. Stromal fibroblasts present in invasive human breast carcinomas promote tumor growth and angiogenesis through elevated SDF-1/CXCL12 secretion. *Cell.* 121:335–348. http://dx.doi.org/10.1016/j.cell.2005.02.034

Oudin, M.J., O. Jonas, T. Kosciuk, L.C. Broye, B.C. Guido, J. Wyckoff, D. Riquelme, J.M. Lamar, S.B. Asokan, C. Whittaker, et al. 2016. Tumor Cell-Driven Extracellular Matrix Remodeling Drives Haptotaxis during Metastatic Progression. *Cancer Discov.* 6:516–531. http://dx.doi.org/10.1158/2159-8290.CD-15-1183

Özdemir, B.C., T. Pentcheva-Hoang, J.L. Carstens, X. Zheng, C.C. Wu, T.R. Simpson, H. Laklai, H. Sugimoto, C. Kahlert, S.V. Novitskiy, et al. 2014. Depletion of carcinoma-associated fibroblasts and fibrosis induces immunosuppression and accelerates pancreas cancer with reduced survival. *Cancer Cell.* 25:719–734. (published erratum appears in *Cancer Cell*. 2015. 28:6) http://dx.doi.org/10.1016/j.ccr.2014.04.005

Poincloux, R., F. Lizárraga, and P. Chavrier. 2009. Matrix invasion by tumour cells: a focus on MT1-MMP trafficking to invadopodia. *J. Cell Sci.* 122:3015–3024. http://dx.doi.org/10.1242/jcs.034561

Provenzano, P.P., K.W. Eliceiri, J.M. Campbell, D.R. Inman, J.G. White, and P.J. Keely. 2006. Collagen reorganization at the tumor-stromal interface facilitates local invasion. *BMC Med.* 4:38. http://dx.doi.org/10.1186/1741-7015-4-38

Rahman, S., Y. Patel, J. Murray, K.V. Patel, R. Sumathipala, M. Sobel, and E.S. Wijelath. 2005. Novel hepatocyte growth factor (HGF) binding domains on fibronectin and vitronectin coordinate a distinct and amplified Met-integrin induced signalling pathway in endothelial cells. *BMC Cell Biol.* 6:8. http://dx.doi.org/10.1186/1471-2121-6-8

Rhim, A.D., P.E. Oberstein, D.H. Thomas, E.T. Mirek, C.F. Palermo, S.A. Sastra, E.N. Dekleva, T. Saunders, C.P. Becerra, I.W. Tattersall, et al. 2014. Stromal elements act to restrain, rather than support, pancreatic ductal adenocarcinoma. *Cancer Cell.* 25:735–747. http://dx.doi.org/10.1016/j.ccr.2014.04.021

Riching, K.M., B.L. Cox, M.R. Salick, C. Pehlke, A.S. Riching, S.M. Ponik, B.R. Bass, W.C. Crone, Y. Jiang, A.M. Weaver, et al. 2014. 3D collagen alignment limits protrusions to enhance breast cancer cell persistence. *Biophys. J.* 107:2546–2558. http://dx.doi.org/10.1016/j.bpj.2014.10.035

Roca-Cusachs, P., A. del Rio, E. Puklin-Faucher, N.C. Gauthier, N. Biais, and M.P. Sheetz. 2013. Integrin-dependent force transmission to the extracellular matrix by α-actinin triggers adhesion maturation. *Proc. Natl. Acad. Sci. USA.* 110:E1361–E1370. http://dx.doi.org/10.1073/pnas.1220723110

Rossier, O., V. Octeau, J.B. Sibarita, C. Leduc, B. Tessier, D. Nair, V. Gatterdam, O. Destaing, C. Albigès-Rizo, R. Tampé, et al. 2012. Integrins β1 and β3 exhibit distinct dynamic nanoscale organizations inside focal adhesions. *Nat. Cell Biol.* 14:1057–1067. http://dx.doi.org/10.1038/ncb2588

Sanz-Moreno, V., C. Gaggioli, M. Yeo, J. Albrengues, F. Wallberg, A. Viros, S. Hooper, R. Mitter, C.C. Féral, M. Cook, et al. 2011. ROCK and JAK1 signaling cooperate to control actomyosin contractility in tumor cells and stroma. *Cancer Cell.* 20:229–245. http://dx.doi.org/10.1016/j.ccr.2011.06.018

Schiller, H.B., M.R. Hermann, J. Polleux, T. Vignaud, S. Zanivan, C.C. Friedel, Z. Sun, A. Raducanu, K.E. Gottschalk, M. Théry, et al. 2013. β1- and αv-class integrins cooperate to regulate myosin II during rigidity sensing of fibronectin-based microenvironments. *Nat. Cell Biol.* 15:625–636. http://dx.doi.org/10.1038/ncb2747

von Wichert, G., G. Jiang, A. Kostic, K. De Vos, J. Sap, and M.P. Sheetz. 2003. RPTP-α acts as a transducer of mechanical force on α_v/β_3-integrin–cytoskeleton linkages. *J. Cell Biol.* 161:143–153. http://dx.doi.org/10.1083/jcb.200211061

Wilson, E., K. Sudhir, and H.E. Ives. 1995. Mechanical strain of rat vascular smooth muscle cells is sensed by specific extracellular matrix/integrin interactions. *J. Clin. Invest.* 96:2364–2372. http://dx.doi.org/10.1172/JCI118293

Wirtz, D., K. Konstantopoulos, and P.C. Searson. 2011. The physics of cancer: the role of physical interactions and mechanical forces in metastasis. *Nat. Rev. Cancer.* 11:512–522. http://dx.doi.org/10.1038/nrc3080

Wolanska, K.I., and M.R. Morgan. 2015. Fibronectin remodelling: cell-mediated regulation of the microenvironment. *Biochem. Soc. Trans.* 43:122–128. http://dx.doi.org/10.1042/BST20140313

Wolf, K., M. Te Lindert, M. Krause, S. Alexander, J. Te Riet, A.L. Willis, R.M. Hoffman, C.G. Figdor, S.J. Weiss, and P. Friedl. 2013. Physical limits of cell migration: Control by ECM space and nuclear deformation and tuning by proteolysis and traction force. *J. Cell Biol.* 201:1069–1084. http://dx.doi.org/10.1083/jcb.201210152

Zaidel-Bar, R., R. Milo, Z. Kam, and B. Geiger. 2007. A paxillin tyrosine phosphorylation switch regulates the assembly and form of cell-matrix adhesions. *J. Cell Sci.* 120:137–148. http://dx.doi.org/10.1242/jcs.03314